

Investigating self-supervised representations for audio-visual deepfake detection

Dragos-Alexandru Boldisor^{*1,2} Stefan Smeu^{*1} Dan Oneata^{2,1} Elisabeta Oneata¹
¹Bitdefender ²POLITEHNICA Bucharest

{ssmeu, dboldisor, eoneata}@bitdefender.com dan.oneata@gmail.com

Abstract

Self-supervised representations excel at many vision and speech tasks, but their potential for audio-visual deepfake detection remains underexplored. Unlike prior work that uses these features in isolation or buried within complex architectures, we systematically evaluate them across modalities (audio, video, multimodal) and domains (lip movements, generic visual content). We assess three key dimensions: detection effectiveness, interpretability of encoded information, and cross-modal complementarity. We find that most self-supervised features capture deepfake-relevant information, and that this information is complementary. Moreover, models primarily attend to semantically meaningful regions rather than spurious artifacts (such as the leading silence). Among the investigated features, audio-informed representations generalize best and achieve state-of-the-art results. However, generalization to realistic in-the-wild data remains challenging. Our analysis indicates this gap stems from intrinsic dataset difficulty rather than from features latching onto superficial patterns. Project webpage: <https://bit-ml.github.io/ssr-dfd>.

1. Introduction

Generative models now produce text, images, audio, video, all rivaling human creations. This progress brings a new challenge: detect whether content is authentic or machine-generated (deepfake). Reliable detection prevents obvious risks such as disinformation and fraud, but also serves a simple need: users want to know what they can trust. We tackle the detection problem in the video domain, the internet’s most consumed medium and, in particular, we focus on people speaking, the most consequential form of deepfakes.

Many approaches are being continuously proposed for the task of audio-visual deepfake detection: these range from powerful discriminative classifiers [39, 42, 55, 83] to techniques that exploit inconsistencies between modalities [19, 43, 44, 66]. Yet, the backbone features underlying

^{*}Equal contribution.

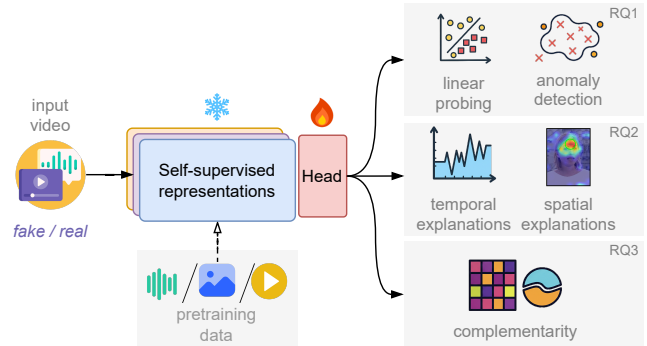


Figure 1. We evaluate a wide array of self-supervised representations for audio-visual deepfake detection. We design a multi-faceted evaluation to understand their: (i) usefulness and robustness (via linear probing and anomaly detection), (ii) focus and interpretability (via temporal and spatial explanations), and (iii) complementarity (via correlation and fusion analyses).

these models often determine their effectiveness. Recent work shows strong results of self-supervised learning in this context: image-based detectors benefit from CLIP [17, 57], audio-based detectors from Wav2Vec2 [60, 82], and audio-visual models from AV-HuBERT [44, 65]. The self-supervised representations capture rich, modality-specific structure without requiring task-specific supervision, making them especially attractive for deepfake detection.

In this paper, we evaluate for the first time a wide range of self-supervised features (audio-only, image-only, multi-modal) for the task of audio-visual deepfake detection. Our aim is to understand what these features capture and how they contribute to detection performance. We center our work around three research questions:

1. **How useful are self-supervised features for deepfake detection?** Do they generalize across domains and to the related task of anomaly detection?
2. **Where do self-supervised features look?** Does the model attend to the manipulated regions? Does it align with human annotations?
3. **How complementary are different features?** If multiple feature types succeed at detection, do they rely on similar

cues or do they encode distinct information?

To answer these questions, we start by adapting linear probing [3, 7, 28] to the video domain. By keeping the classifier minimal, we can directly measure the information already encoded in the feature representations. We evaluate both on standard scientific datasets [8, 32, 47], but also on challenging in-the-wild data [11], assessing both in-domain and out-of-domain performance.

However, prior work has warned that even subtle distribution shifts between real and fake samples can be exploited by classifiers, leading to spurious correlations [10, 36, 52, 73]. Worse still, such spurious cues may persist across datasets, yielding overly optimistic results. We therefore propose a multi-faceted evaluation suite (Fig. 1) that goes beyond standard supervised testing and more directly tests whether the representations capture meaningful forensic cues.

First, we assess feature quality via the proxy task of anomaly detection. By training only on real samples, we break the real-fake asymmetry and avoid relying on spurious cues. We consider two approaches: (i) density estimation via next-token prediction, and (ii) audio-video synchronization, which measures cross-modal alignment between representations. Second, to further probe model behavior, we extract implicit localizations from the classifier. We apply temporal and spatial explainability methods and test whether the resulting explanations align with temporal manipulations [8] and human annotations [26], respectively. Finally, we examine whether the representations capture different information by measuring the correlation between their predictions and the downstream performance of their combination.

Our main findings are as follows: 1. Many of the investigated features obtain strong in-domain detection performance. Audio-informed representations generalize best and achieve state-of-the-art results. 2. Training only on real data helps identify features that rely solely on spurious cues, but remain less effective for deepfake detection than supervised learning. 3. Temporal explanations indicate that many features capture meaningful cues, even in the presence of spurious correlations. Spatial explanations are plausible and partially match human annotations. 4. Visual representations are more complementary than audio ones. Combining representations yields gains that tend to increase with complementarity.

2. Related work

Self-supervised learning (SSL) learns powerful representations by solving pretext tasks on large-scale unlabeled data [6]. These representations transfer effectively to many downstream tasks, such as classification or anomaly detection. In the **visual** domain [78], many approaches use contrastive learning between images and their augmented versions [13, 24] or images and their captions [29, 64]. Al-

ternatives include masked image modeling [25] or discriminative self-distillation [59, 71]. For video, spatio-temporal information is used to build SSL representations [63, 77]. In the **audio** domain [46], Wav2Vec [4, 5] and HuBERT [27] introduced predictive coding and masked prediction for speech signals, significantly improving ASR with limited labeled data. For **audio-visual** data, AV-HuBERT [70] extends HuBERT to learn joint speech-lip representations.

Self-supervised features for deepfake detection have shown great promise. In the **visual** domain, a frozen CLIP backbone with only a linear layer offers strong generalization [57]. As such, CLIP is arguably the most popular SSL encoder for image deepfake detection [17, 33, 40, 45, 65, 72, 74, 90], but others have explored other vision-language encoders (e.g., BLIP2 [31, 65], InstructBLIP [12]) or vision-only models (e.g., DINO [54], MoCo [85]). Similarly, the **audio** deepfake detection community has adopted large SSL representations, with most popular ones being Wav2Vec [50, 60, 61, 75, 79, 82, 84], followed by HuBERT [34] and WavLM [16, 21]. For **audio-visual** deepfake detection, AV-HuBERT representations have shown strong performance not only in a fully supervised paradigm [69], but also in zero-shot [44, 65] or unsupervised [73] settings.

Audio-visual deepfake detection typically exploits cross-modal inconsistencies. Early methods targeted semantic mismatches, such as phoneme-viseme inconsistencies [2] or emotional incongruences between speech and facial expressions [51]. More recent work detects forgeries by measuring misalignment between dense audio-visual representations [19, 43, 44, 73]. These representations are typically learned in a self-supervised manner, either trained from scratch [19, 58, 83, 87] or obtained from pretrained models [37, 39, 44, 65]. In contrast to these studies, we provide a comprehensive evaluation across multiple representations rather than focusing on a single one.

3. Methodology

Deepfake detection is a binary classification task that attempts to map an input video \mathbf{x} to a binary label y (1 if the video is fake and 0 otherwise). We build deepfake detection models that rely mostly on self-supervised features and learn a minimal amount of parameters on top of these features. This approach is related to linear probing [3, 7, 28] and it allows us to assess the quality of the representations in a comparable setting. While more complex models could be explored for downstream performance, prior work shows that simple linear models often suffice [57, 60].

The model has three steps: 1. extract locally temporal features (e.g., an embedding $\phi(\mathbf{x})_t$ for each frame t); 2. apply a learnable linear classifier \mathbf{w} ; 3. aggregate the predictions using a pooling function (such as log-sum-exp). Formally,

the per-video score s is defined as:

$$s(\mathbf{x}; \mathbf{w}) = \log \sum_t \exp \{ \mathbf{w}^\top \phi(\mathbf{x})_t \} \quad (1)$$

Since the log-sum-exp approximates the max function, the model learns to predict that a video is fake if only a single region of the model is fake. Note that even if the model uses locally temporal features, many of the representations we test encode global temporal information (see Tab. 1). The parameters of the linear layer are trained by minimizing the cross-entropy loss on video-level labels. See App. A for more implementation details.

3.1. Explanations

To understand how deepfake detection classifiers make decisions, we generate both temporal and spatial explanations.

Temporal explanations. Since the pooling function (log-sum-exp) is a simple transformation of its inputs, the final video-level prediction can be regarded as an aggregation of local frame-level predictions. We therefore compute per-frame scores $s_t = \mathbf{w}^\top \phi(\mathbf{x})_t$ to measure which time segments contribute most to the final prediction.

Spatial explanations. Given that the per-frame classifier is linear, we can further decompose each frame-level decision into patch-level contributions. If the per-frame feature is computed by averaging patch features, we can propagate the linear classifier down to the patch level [88]. If non-linear aggregation is used, we instead apply Grad-CAM [68] to obtain patch-level relevance maps.

Evaluation. We compare the resulting temporal and spatial explanations against the annotated extent of local manipulations or human annotations. Since the classifiers are trained only with video-level supervision, this comparison also serves as a form of weakly-supervised localization.

3.2. Proxy tasks: Anomaly detection

Instead of training a binary classifier, which risks latching onto spurious features, we explore two anomaly detection tasks that rely on real data only: next-token prediction and audio-video synchronization. These are proxy tasks because they do not address deepfake detection directly; rather, they model the distribution of real data, and assume that deviations from this distribution indicate fakes. Both approaches have shown promising performance [19, 73].

Next-token prediction models the probability of the next frame’s representation \mathbf{x}_t given the previous frames $\mathbf{x}_1, \dots, \mathbf{x}_{t-1}$. The assumption is that frames that cannot be predicted well are more likely to indicate manipulations. We use a decoder-only Transformer trained with the mean squared error on real videos. At test time, the model predicts each frame given its corresponding history, and we obtain a

per-video fakeness score as the maximum frame-level mean squared error. The models’ architecture has 4 layers each containing 4 heads, a feature dimension of 512 and a feed-forward dimension of 1024. In order to match the input encoding dimension, projection layers are applied before and after the Transformer.

Audio-video synchronization models how well the audio and video frame-level representations match. The assumption is that mismatches between the two modalities indicate manipulations. We use an alignment network Φ [73], where L2-normalized audio features \mathbf{a} and visual features \mathbf{v} are concatenated and passed through a four-layer MLP with Layer Normalization and ReLU activations. The network is trained to maximize the probability that an audio frame \mathbf{a}_i aligns with its corresponding video frame \mathbf{v}_i , rather than with neighboring frames $N(i)$:

$$p(\mathbf{v}_i | \mathbf{a}_i) = \frac{\exp(\Phi(\mathbf{a}_i, \mathbf{v}_i))}{\sum_{k \in N(i)} \exp(\Phi(\mathbf{a}_i, \mathbf{v}_k))}. \quad (2)$$

At test time, the per-frame alignment scores $\Phi(\mathbf{a}_i, \mathbf{v}_i)$ are inverted to estimate fakeness, and then pooled across the video using a log-sum-exp operator to produce the final detection score.

4. Models

We study a wide range of self-supervised representation: from models trained on audio-visual data to models trained on visual-only or audio-only data. Tab. 1 summarizes the models used in the paper. The exact model checkpoints are in App. B.

4.1. Vision-only encoders

We consider three models whose pretraining data range from faces to generic images or video. **CLIP** [64] is an image-text model trained on general images collected from the internet. We use the ViT/L-14 model, and take the CLS token produced by the image encoder. **FSFM** [80] is a foundation model trained on faces for reconstruction. FSFM uses a ViT/B-14 model and produces frame-level embeddings by average pooling patch embeddings. **VideoMAE** [77] is a vision transformer model trained to reconstruct patches of generic video. It extracts features from spatio-temporal patches of size $2 \times 16 \times 16$ in a window of 16 frames and with stride 16. We discard the last window if its length is shorter than 16 frames.

4.2. Audio-only encoders

Wav2Vec XLS-R 2B [5] is a speech model trained on 436k hours of multilingual audio. It uses a convolutional encoder followed by a transformer, and it is trained to match contextual representations with corresponding local quantized representations. We use the final-layer features; these are

Model	Input		Pretraining				Params.	Dim.
	Modality	Context	Modality	Content	Dataset			
<i>Audio features</i>								
Wav2Vec XLS-R 2B	audio	full	audio	speech	MLS and others	2159M	1920	
Auto-AVSR (ASR)	audio	full	audio	speech	LRS3	243M	768	
AV-HuBERT (A)	audio	full	multimodal	lips + speech	VoxCeleb, LRS3	310M	1024	
BRAVE _n (A)	audio	full	multimodal	lips + speech	VoxCeleb2 (en), LRS3, AVS	332M	1024	
<i>Visual features</i>								
CLIP VIT-L/14	visual	frame	visual (images)	generic	WebImageText	303M	768	
FSFM	visual	frame	visual (video)	faces	VGGFace2	86M	768	
Video-MAE-large	visual	chunk	visual (video)	generic	Kinetics-400	303M	1024	
Auto-AVSR (VSR)	visual	full	visual (video)	lips	LRS3	250M	768	
AV-HuBERT (V)	visual	full	multimodal	lips + speech	VoxCeleb, LRS3	322M	1024	
BRAVE _n (V)	visual	full	multimodal	lips + speech	VoxCeleb2 (en), LRS3, AVS	339M	1024	
<i>Audio-visual features</i>								
Auto-AVSR	multimodal	full	multimodal	lips + speech	LRS3	443M	768	
AV-HuBERT	multimodal	full	multimodal	lips + speech	VoxCeleb, LRS3	322M	1024	

Table 1. Overview of the models studied in the paper. The modality from which features are extracted (“input modality”) can differ from the modality used at training (“pretraining modality”). “Context” indicates whether the embeddings are contextual (extracted from the full input—audio or video) or local (extracted from a frame or chunk).

extracted every 20 ms (50 Hz), but to match 25 FPS video, we concatenate pairs of consecutive feature vectors.

4.3. Audio-visual encoders

We consider three audio-visual models; all are trained on face video and extract visual features from lip regions. **AV-HuBERT** [70] is a Transformer that jointly encodes audio and visual inputs and is trained with masked multimodal cluster prediction. We obtain modality-specific representations by masking one stream: for AV-HuBERT (A) we mask visual input, and for AV-HuBERT (V) we mask audio input. **BRAVE_n** [23] uses a two-tower Transformer architecture pretrained in a cross-modal teacher–student setup: the student predicts from masked inputs to match the teacher’s prediction from the original data. We use the two student encoders, fine-tuned for ASR and VSR, respectively. **Auto-AVSR** [48, 49] is an audio-visual speech recognition model.¹ Its encoders use the Conformer architecture [20]. We obtain modality-specific representations from independently trained models: the visual-only encoder trained for VSR, and the audio-only encoder trained for ASR.

5. Experimental setup

5.1. Datasets

We consider four audio-visual datasets varying in terms of generation methods, manipulation scope (full or local), source domain (academic or real-world).

¹Auto-AVSR is not an SSL model, but we include it for completeness.

FakeAVCeleb [32] (FAVC) contains 500 real videos from VoxCeleb2 [15] and 19.5k fake videos, generated using face swapping methods (Faceswap [38]; FSGAN [56]), lip-syncing (Wav2Lip [62]), and voice cloning (SV2TTS [30]). Since the dataset does not come with a predefined split, in line with previous works we split the dataset in 70% (training and validation) and 30% testing samples.

AV-Deepfake1M [8] (AV1M) comprises over one million videos of approximately 2k subjects. The videos are locally manipulated by modifying their transcripts with ChatGPT. Corresponding fake video segments are generated with TalkLip [81], while fake audio segments are generated with VITS [35] or YourTTS [9]. We subsample the original training set for training and validation data, and evaluate on 5133 samples taken from the original validation set (see App. A).

DeepfakeEval 2024 [11] (DFE-2024) is a real-world dataset collected from 88 websites through social media and the [TrueMedia.org](https://www.truemedia.org) platform. The dataset contains deepfakes circulating online in 2024 across multiple media (audio, video, images) and in 52 different languages; the types of manipulations are unknown. We use the video subset, totaling 45 hours, which we preprocess into single-speaker segments (see App. C). This process yields for 70 real and 507 fake samples for test, averaging 14.06 seconds.

AVLips [47] (AVL) contains 3.4k real and 4.2k fake samples. The real videos are sourced from LRS3 [1], FF++ [67] and DFDC [18], while fake videos are generated using MakelItTalk [89], Wav2Lip [62], TalkLip [81] or SadTalker [86]. We evaluate on the whole dataset.

5.2. Evaluation and baselines

Classification. To measure how well fake samples can be distinguished from real ones, we report the area under receiver operator characteristic curve (AUC). This metric has the advantages of being threshold-independent and having a clear baseline: a random model achieves 50% AUC, regardless of the class distribution. We also report average precision results in App. E.1, Tab. 5 & Tab. 6. For a fair evaluation, only fake samples with both audio and visual manipulations are considered, where this information is available.

Temporal localization. We evaluate how well temporal explanations align with ground-truth annotations. For this, we consider the videos from the AVIM test set that contain at least one fake segment, and compute a localization score per video. The localization score is computed in terms of AUC by treating each frame as an independent sample: the model’s frame-level score serves as the prediction, while annotated fake segment specifies the groundtruth label. The final localization score is the average of the AUC values across all fake test videos.

Baselines. To understand how much information is implicitly encoded in the architecture, we report results of an untrained (randomly initialized) AV-HuBERT model. To further contextualize the results, we include five state-of-the-art approaches: AVAD [19], AVFF [58], SpeechForensics [44], AuViRe [41], RealForensics [22]. For AVFF we use the unofficial open source implementation² and finetune the Kinetics400 checkpoint on the same datasets as the linear probes. For the rest we use the pretrained models. For more details, see App. D.

6. Experimental results

We first evaluate how useful are the representations for both the direct task of deepfake detection, as well as the proxy task of anomaly detection (Sec. 6.1). Then we evaluate the models in terms of what they look at when making their decision (Sec. 6.2). Finally, we quantify how different the deepfake information encoded by the representations is (Sec. 6.3).

6.1. How useful are the representations?

Tab. 2 shows the main results: linear probes results across the selected self-supervised features and across multiple combinations of in-domain and out-of-domain datasets.

Many features can encode deepfake information. We observe strong in-domain results on the scientific datasets (cols. A and C), which show that many representations are able to encode the subtle information needed to differentiate between real and fake samples. This is especially remarkable for the AVIM dataset, which has only short temporal

manipulations. Interestingly, the deepfake information can be picked from different angles: from audio (Wav2Vec2, AV-HuBERT (A)), from motion information (Video-MAE), from static vision content (CLIP).

Audio-informed features generalize best. On FAVC and AVIM (cols. A:D), audio representations perform best. On AVLips and DFE-2024 (cols. E:F), which lack or have incomplete audio manipulations, audio-informed visual representations (AV-HuBERT (V) and BRAVEN (V)) are best. These models, albeit simple, achieve state-of-the-art performance (Tab. 3). Among existing methods, only SpeechForensics approaches this performance; but as discussed in App. E.2, this is because it relies on similar features (AV-HuBERT) and formulates detection as anomaly detection. We also experimented with a more powerful backend classifier (a transformer) and observed similar results (App. E.3), suggesting that features are more important than the classifier.

In-the-wild data is not only different, but also harder. Generalization to DFE-2024 (cols. H:I) is poorer than to other datasets (cols. B, D:F): the best out-of-domain result on DFE-2024 reaches only 76.0% AUC, achieved by BRAVEN (V) (cell I12). While this gap may reflect differences between datasets (in terms of content or artifacts), it also indicates that DFE-2024 is intrinsically more difficult [53]: even the best in-domain result is at only 75.5% AUC (cell G12).

Random features are not random. Surprisingly, results of the randomly-initialized models (rows 1:2) are well above random chance (50% AUC). This indicates that the architectures can implicitly encode information that is discriminative. But how useful is this information really? Results from Sec. 6.2 suggest that random features encode spurious cues, such as the leading silence [36, 73], which explains the better performance of the random audio model compared to its visual counterpart.

Anomaly detection offers robustness, but only certain feature combinations work. Tab. 4 presents deepfake detection performance for models trained on the two anomaly detection tasks (next-token prediction and synchronization), along with cross-domain supervised results. As just seen, supervised models can perform well even when trained on features from random models. When these random features are used for the two proxy anomaly detection tasks, performance drops sharply: down to chance level for synchronization and to moderate values for next-token prediction. This confirms that the unsupervised methods are more robust: unlike supervised classifiers, they do not exploit spurious correlations that random features may inadvertently encode. However, to achieve reasonable anomaly detection results, specific feature combinations are required. For next-token prediction, AV-HuBERT (A) features are essential: they perform best

²<https://github.com/JoeLeelyf/OpenAVFF>

Model	Modality	A	B	C	D	E	F	G	H	I	J
		Test on FAVC		Test on AV1M		Test on AVLips		Test on DFE-2024			
		FAVC	AV1M	AV1M	FAVC	FAVC	AV1M	DFE	FAVC	AV1M	mean
		↓	↓	↓	↓	↓	↓	↓	↓	↓	OOD
1 AV-HuBERT (A) random	audio	99.8	97.8	98.8	92.0	50.9	51.9	53.4	41.9	46.4	63.5
2 AV-HuBERT (V) random	visual	83.8	52.5	50.2	49.3	60.4	53.8	56.8	60.6	54.0	55.1
3 Wav2Vec2	audio	100	99.9	100	96.6	51.3	56.3	58.7	62.3	58.6	70.8
4 Auto-AVSR (ASR)	audio	99.7	76.0	96.4	50.3	52.9	49.6	63.5	49.4	47.5	54.3
5 AV-HuBERT (A)	audio	100	100	100	99.0	50.0	57.2	65.8	49.1	48.3	67.3
6 BRAVEEn (A)	audio	100	99.7	99.9	89.4	44.5	47.6	67.8	64.2	54.6	66.7
7 CLIP VIT-L/14	visual	99.8	95.2	96.5	71.1	60.3	53.3	73.9	55.6	43.5	63.2
8 FSFM	visual	97.1	40.9	95.3	52.7	84.3	36.8	71.7	71.8	43.5	55.0
9 Video-MAE-large	visual	100	70.4	99.8	60.0	71.3	47.2	54.5	45.6	39.3	55.6
10 Auto-AVSR (VSR)	visual	97.8	77.5	59.0	51.3	83.3	70.1	64.3	48.7	56.1	64.5
11 AV-HuBERT (V)	visual	100	95.5	93.7	64.1	98.3	90.5	72.1	63.7	67.7	80.0
12 BRAVEEn (V)	visual	100	98.8	93.0	66.3	98.9	96.7	75.5	70.8	76.0	84.6
13 Auto-AVSR	audio-visual	94.7	68.3	91.6	53.2	59.6	54.6	61.2	43.0	49.2	54.7
14 AV-HuBERT	audio-visual	100	99.5	99.9	94.5	78.5	84.4	70.4	58.2	54.3	78.2

Table 2. Area under curve (AUC, %) of linear probes trained on different representations and evaluated in (columns A, C, G) and out of domain (other columns). AVLips and DFE-2024 lack or have incomplete audio manipulations, hence the gray values for the audio features.

Method	Sup?	Test dataset				Average	
		AV1M	FAVC	AVL	DFE	All4	Last3
<i>Self-supervised features (best in each modality) and linear probing</i>							
Wav2Vec2 (A)	✓	100	99.9	56.3	58.6	78.7	71.6
BRAVEEn (V)	✓	93.0	98.8	96.7	76.0	91.1	90.5
AV-HuBERT (AV)	✓	99.9	99.5	84.4	54.3	84.5	79.4
<i>State-of-the-art approaches: Supervised and unsupervised</i>							
AVFF [58]	✓	98.0	89.2	53.9	58.1	74.8	67.1
AuViRe [†] [41]	✓	100	88.1	72.4	63.8	81.1	74.7
RealForensics [‡] [22]	✓	60.7	89.1	76.8	74.4	75.2	80.1
AVAD [19]		52.9	95.2	73.2	64.8	71.5	77.7
SpeechForensics [44]		68.1	100	92.7	75.6	84.1	89.4

Table 3. Comparison to state of the art. AUC (%) when training on the AV1M dataset (23k samples). We report average score across all datasets (All4) and without AV1M (Last3). Legend: † trained on the full AV1M training set (746k samples); ‡ trained on FF++ [67].

individually and substantially improve performance when combined with others. For synchronization, however, AV-HuBERT (V) features are crucial; this contrasts with CLIP or random features, which are insufficient. The only setting that comes close to the supervised model is the synchronization model on AV-HuBERT (A) + AV-HuBERT (V). Taken together, the results indicate that robustness in anomaly detection depends on selecting features that capture the temporal dynamics necessary to align and compare audio-visual streams effectively.

Model	AV1M			FAVC		
	Sup.	NTP	Sync.	Sup.	NTP	Sync.
<i>Single features</i>						
AV-HuBERT (A)	99.0	90.6	N/A	100	80.5	N/A
Wav2Vec2	96.6	56.6	N/A	99.9	59.4	N/A
AV-HuBERT (V)	64.1	46.1	N/A	95.5	55.3	N/A
CLIP	71.1	47.3	N/A	95.2	60.2	N/A
<i>Combination of features</i>						
AV-H (A + V) random	74.0	64.4	50.0	95.0	75.4	50.3
AV-H (A + V)	97.2	84.5	87.3	100	91.2	96.3
AV-H (A) + CLIP	99.0	86.9	50.0	100	79.6	54.4
W2V2 + AV-H (V)	96.2	60.6	86.5	100	79.4	94.6
W2V2 + CLIP	97.1	57.2	49.7	100	69.8	21.7

Table 4. AUC performance (%) on AV1M and FAVC of supervised (sup.) and anomaly detection models: next-token prediction (NTP) and audio-video synchronization (sync.). Supervised models are trained cross-domain (FAVC→AV1M and AV1M→FAVC, respectively), while anomaly detection models are trained on real data only (a subset of VoxCeleb). Supervised models of feature combinations use late fusion (average of predictions).

6.2. What do models look at?

Localization of temporal explanations: Audio models pick leading silence, but also useful artifacts. Fig. 2 shows the alignment between the temporal explanations and local manipulations from AV1M. We see that many features still produce strong results (localization performance is close to that of classification), indicating that linear probes ex-

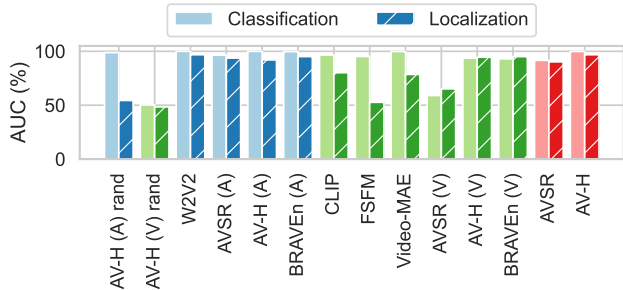


Figure 2. Temporal localization of explanations (solid bars) and deepfake classification (hatched bars) on AV1M. Colors indicate modality: blue (audio), green (visual), red (audio-visual).

tract reasonable information from the representations. Large performance drops appear only for the random models, confirming that they rely on spurious cues, and for FSFM, where inspection did not reveal a visible bias. Audio models show strong performance, but qualitative examples in Fig. 3 indicate that they do attend to leading silence. Despite this, they also focus on the manipulated regions, retaining good localization performance; interestingly, Wav2Vec2 seems to select transition boundaries. Among the four models shown, AV-HuBERT (V) produces the cleanest predictions, while CLIP is the noisiest—its activations often fire on blurry frames, although this is difficult to quantify since scores fluctuate even between adjacent, visually similar frames.

Spatial alignment to human annotations: CLIP attends to facial artifacts, similarly to humans. We saw that the models find temporarily modified regions. Do they also look at the same artifacts as humans? To answer this question, we analyze the recently introduced ExDDV dataset [26], which provides click annotations indicating where humans identified generation artifacts. We compare these annotations with explanations produced by a CLIP-based model trained on the ExDDV training set (this model achieves 71.3% AUC on the ExDDV test set). We generate explanations for the fake test videos using GradCAM applied to the final LayerNorm layer of the CLIP visual encoder. We quantify the human-machine alignment as the mean absolute error (MAE) between the relative coordinates of human click annotations and the maximum values in the GradCAM attention maps. To contextualize these results, we compare against several baselines: random position within each frame, frame center, face center, and a predictive click model trained on click annotations (the ViT model from [26]).

Fig. 4 (left) presents quantitative results: MAE as a function of the minimum fakeness score. We observe that error decreases with the minimum fakeness score, suggesting better alignment for confident predictions (these predictions are also correct, since we consider only fake samples). The variance increases correspondingly due to fewer samples

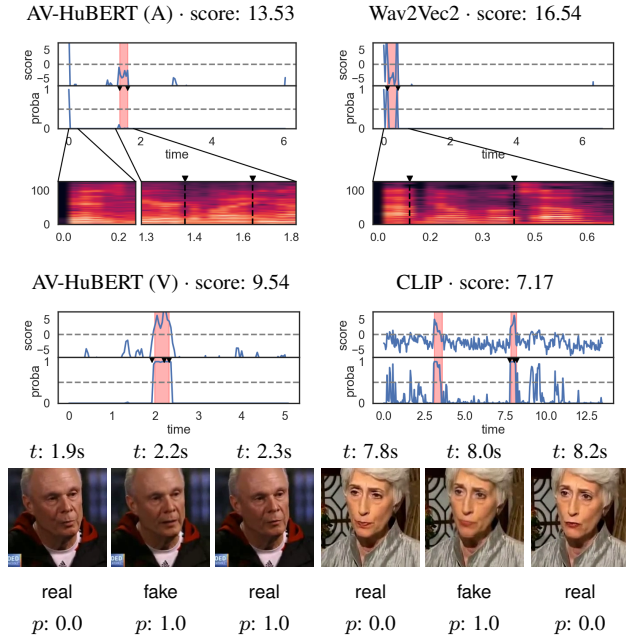


Figure 3. Temporal explanations of the top video predictions for four SSL representations. The predictions are given in terms of unnormalized scores (logits) and probabilities. Red regions indicate fake segments, and gray dashed lines correspond to the decision boundary (0.5 probability). For audio models we show Mel spectrograms; for vision models we show three frames (corresponding to the triangle markers on the line plot).

exceeding the higher score thresholds. Compared to baseline methods, the explanations achieve better alignment than frame center (0.117 MAE) or random locations (0.270 MAE, not shown). However, alignment remains lower than what a predictive model achieves (0.055 MAE). Notably, the predictive click model performs only marginally better than face center prediction (0.058 MAE), suggesting that human annotations may not contain substantially more localization information beyond indicating that artifacts occur somewhere on the face. Fig. 4 (right) shows qualitative results. In these samples, most model predictions concentrate on the forehead region, while human annotations focus on eyes and lips. Crucially, the model appears to avoid relying on spurious background features, with explanations consistently concentrating on facial regions.

6.3. How complementary are the representations?

To understand how the different self-supervised representations relate, we examine two aspects. First, we measure the correlation between predictions produced by pairs of models. This evaluation provides insight into the similarity of their learned decision boundaries. Second, we evaluate downstream performance when combining multiple models. This offers a more direct assessment of the feature combination

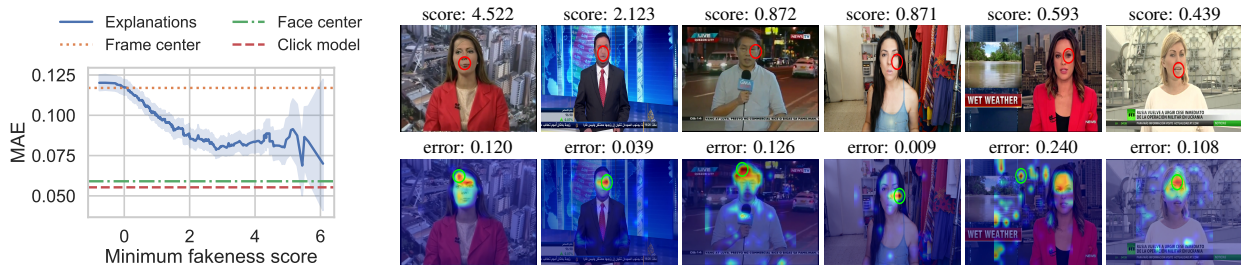


Figure 4. Alignment of spatial explanations to human annotations. *Left*: Alignment error in terms of mean absolute error (MAE) as a function of the model confidence (fakeness score). The explanations align better to human annotations as the model is more confident in its predictions. *Right*: Qualitative samples human annotation shown as the center of the red circle on top frame, and explanation of the CLIP-based model shown on bottom frame (maximum value indicated by the green circle).

	Model correlation					AUC	Relative improvement (%)				
W2V2	100.0	66.2	26.9	5.6	21.5	99.9	0.0	0.1	0.1	-0.2	0.1
AV-H (A)	66.2	100.0	31.2	9.6	24.4	100.0	0.0	0.0	0.0	-0.2	0.0
AV-H (V)	26.9	31.2	100.0	9.7	19.4	95.5	4.7	4.6	0.0	-5.0	2.9
V-MAE	5.6	9.6	9.7	100.0	33.5	70.4	41.6	41.8	28.9	0.0	31.9
CLIP	21.5	24.4	19.4	33.5	100.0	95.2	5.0	5.0	3.3	-2.5	0.0
	W2V2	AV-H (A)	AV-H (V)	V-MAE	CLIP		W2V2	AV-H (A)	AV-H (V)	V-MAE	CLIP

Figure 5. Correlations between models (left) and downstream performance (right). The downstream performance is presented in absolute values for the unimodal models (AUC column) and as relative improvement for feature combinations. Training was done on AV1M, testing on FAVC.

effectiveness toward our final goal. Results on FAVC are in Fig. 5 and on DFE-2024 in App. E.4, Fig. 7.

Vision models are more complementary than audio ones.

For each pair of models, we generate predictions on a shared test dataset and calculate the Pearson correlation coefficient between their outputs. Fig. 5 (left) shows that the cross-model correlations are generally weak to moderate; this suggests that the embeddings encode different information. The strongest correlations occur within modalities: in particular, audio models (AV-HuBERT (A) and Wav2Vec2) show highest correlation with each other, stronger than the vision counterpart (CLIP and VideoMAE). Notably, AV-HuBERT (V) correlates more strongly with audio models than with other video models. This happens because AV-HuBERT (V) focuses solely on lip movements and is trained jointly with the audio component.

Complementarity helps downstream performance, but there are exceptions. The largest gains from feature combination occur for Video-MAE. This is expected, as Video-

MAE has the lowest performance and thus has the most room for improvement. Also, unsurprisingly, Video-MAE benefits most from audio features, which are both stronger and more complementary than the visual ones. However, among similarly performing features, Video-MAE benefits more from CLIP (with which is more aligned) than from AV-HuBERT (V) (with which is more complementary). This suggests that the impact of feature combination is more nuanced than solely their complementarity.

7. Conclusions

We examined a wide array of self-supervised representations for audio-visual deepfake detection. Many of these features, although complementary, are able to perform strongly in-domain, even on challenging locally manipulated data. The representations that generalize best are audio-informed features; in particular, the visual encoder of BRAVEN achieves state-of-the-art results, outperforming more complex approaches. Audio-only features also perform strongly, but only when datasets contain speech-level manipulations.

A surprising finding was that randomly initialized features can achieve strong performance and even generalize across datasets. This observation suggests that standard supervised evaluation can be driven by dataset shortcuts. Indeed, by considering a multifaceted evaluation protocol (anomaly detection, temporal and spatial alignment), we are able to expose such failure modes and show that random features are not aligned with groundtruth manipulations.

Limitations. There remains a gap towards real-world deepfake detection: neither the tested representations nor existing approaches generalize well to such data. Our results indicated that this limitation persists despite the representations being well aligned to semantic artifacts (temporal and spatial). The likely reason is the difficulty and diversity of the real-world data (*e.g.*, missing modalities, shifts in the video domain). Addressing this challenge will require more specialized solutions that explicitly account for this diversity.

Acknowledgments

We thank the reviewers and area chair for their suggestions. This work was supported in part by the EU Horizon project ELIAS (No.101120237) and by CNCS-UEFISCDI (PN-IV-P7-7.1-PTE-2024-0600 and PN-IV-P2-2.1-TE-2023-1632).

References

- [1] Triantafyllos Afouras, Joon Son Chung, and Andrew Zisserman. LRS3-TED: A large-scale dataset for visual speech recognition, 2018. 4
- [2] Shruti Agarwal, Hany Farid, Ohad Fried, and Maneesh Agrawala. Detecting deep-fake videos from phoneme-viseme mismatches. In *CVPR*, 2020. 2
- [3] Guillaume Alain and Yoshua Bengio. Understanding intermediate layers using linear classifier probes. In *ICLR Workshop*, 2017. 2
- [4] A. Babu, C. Wang, A. Tjandra, K. Lakhotia, Q. Xu, N. Goyal, K. Singh, Patrick von Platen, Y. Saraf, J. Pino, A. Baevski, A. Conneau, and M. Auli. XLS-R: Self-supervised cross-lingual speech representation learning at scale. In *Interspeech*, 2022. 2
- [5] A. Baevski, Y. Zhou, A. Mohamed, and M. Auli. Wav2vec 2.0: A framework for self-supervised learning of speech representations. In *NeurIPS*, 2020. 2, 3
- [6] Randall Balestriero, Mark Ibrahim, Vlad Sobal, Ari Morcos, Shashank Shekhar, Tom Goldstein, Florian Bordes, Adrien Bardes, Gregoire Mialon, Yuandong Tian, et al. A cookbook of self-supervised learning. *arXiv preprint arXiv:2304.12210*, 2023. 2
- [7] Yonatan Belinkov. Probing classifiers: Promises, shortcomings, and advances. *Computational Linguistics*, 48(1):207–219, 2022. 2
- [8] Zhixi Cai, Shreya Ghosh, Aman Pankaj Adatia, Munawar Hayat, Abhinav Dhall, Tom Gedeon, and Kalin Stefanov. AV-Deepfake1M: A large-scale LLM-driven audio-visual deepfake dataset. In *ACM MM*, 2024. 2, 4
- [9] Edresson Casanova, Julian Weber, Christopher Dane Shulby, Arnaldo Cândido Júnior, Eren Gölge, and Moacir A. Ponti. YourTTS: Towards zero-shot multi-speaker TTS and zero-shot voice conversion for everyone. In *ICML*, 2022. 4
- [10] Lucy Chai, David Bau, Ser-Nam Lim, and Phillip Isola. What makes fake images detectable? Understanding properties that generalize. In *ECCV*, 2020. 2
- [11] Nuria Alina Chandra, Ryan Murtfeldt, Lin Qiu, Arnab Karmakar, Hannah Lee, Emmanuel Tanumihardja, Kevin Farhat, Ben Caffee, Sejin Paik, Changyeon Lee, et al. Deepfake-Eval-2024: A multi-modal in-the-wild benchmark of deepfakes circulated in 2024. *arXiv preprint arXiv:2503.02857*, 2025. 2, 4
- [12] You-Ming Chang, Chen Yeh, Wei-Chen Chiu, and Ning Yu. AntifakePrompt: Prompt-tuned vision-language models are fake image detectors. *arXiv preprint arXiv:2310.17419*, 2023. 2
- [13] Ting Chen, Simon Kornblith, Mohammad Norouzi, and Geoffrey Hinton. A simple framework for contrastive learning of visual representations. In *ICML*, 2020. 2
- [14] Joon Son Chung and Andrew Zisserman. Lip reading in the wild. In *Asian Conference on Computer Vision*, 2016. 13
- [15] J. S. Chung, A. Nagrani, and A. Zisserman. VoxCeleb2: Deep speaker recognition. In *Interspeech*, 2018. 4
- [16] David Combei, Adriana Stan, Dan Oneata, and Horia Cucu. WavLM model ensemble for audio deepfake detection. *arXiv preprint arXiv:2408.07414*, 2024. 2
- [17] Davide Cozzolino, Giovanni Poggi, Riccardo Corvi, Matthias Nießner, and Luisa Verdoliva. Raising the bar of AI-generated image detection with CLIP. In *CVPRW*, 2024. 1, 2
- [18] Brian Dolhansky, Joanna Bitton, Ben Pfau, Jikuo Lu, Russ Howes, Menglin Wang, and Cristian Canton Ferrer. The deepfake detection challenge (DFDC) dataset. *arXiv preprint arXiv:2006.07397*, 2020. 4
- [19] Chao Feng, Ziyang Chen, and Andrew Owens. Self-supervised video forensics by audio-visual anomaly detection. In *CVPR*, 2023. 1, 2, 3, 5, 6, 13
- [20] Anmol Gulati, James Qin, Chung-Cheng Chiu, Niki Parmar, Yu Zhang, Jiahui Yu, Wei Han, Shibo Wang, Zhengdong Zhang, Yonghui Wu, et al. Conformer: Convolution-augmented transformer for speech recognition. In *Interspeech*, 2020. 4
- [21] Yinlin Guo, Haofan Huang, Xi Chen, He Zhao, and Yuehai Wang. Audio deepfake detection with self-supervised wavLM and multi-fusion attentive classifier. In *ICASSP*, 2024. 2
- [22] Alexandros Haliassos, Rodrigo Mira, Stavros Petridis, and Maja Pantic. Leveraging real talking faces via self-supervision for robust forgery detection. In *CVPR*, 2022. 5, 6, 13
- [23] Alexandros Haliassos, Andreas Zinonos, Rodrigo Mira, Stavros Petridis, and Maja Pantic. BRAVEN: Improving self-supervised pre-training for visual and auditory speech recognition. In *ICASSP*, 2024. 4
- [24] Kaiming He, Haoqi Fan, Yuxin Wu, Saining Xie, and Ross Girshick. Momentum contrast for unsupervised visual representation learning. In *CVPR*, 2020. 2
- [25] Kaiming He, Xinlei Chen, Saining Xie, Yanghao Li, Piotr Dollár, and Ross Girshick. Masked autoencoders are scalable vision learners. In *CVPR*, 2022. 2
- [26] Vlad Hondru, Eduard Hoge, Darian Onchis, and Radu Tudor Ionescu. ExDDV: A new dataset for explainable deepfake detection in video. *arXiv preprint arXiv:2503.14421*, 2025. 2, 7
- [27] Wei-Ning Hsu, Benjamin Bolte, Yao-Hung Hubert Tsai, Kushal Lakhotia, Ruslan Salakhutdinov, and Abdelrahman Mohamed. HuBERT: Self-supervised speech representation learning by masked prediction of hidden units. *IEEE ACM Trans. Audio Speech Lang. Process.*, 29:3451–3460, 2021. 2
- [28] Dieuwke Hupkes, Sara Veldhoen, and Willem Zuidema. Visualisation and ‘diagnostic classifiers’ reveal how recurrent and recursive neural networks process hierarchical structure. *Journal of Artificial Intelligence Research*, 61:907–926, 2018. 2
- [29] Chao Jia, Yinfei Yang, Ye Xia, Yi-Ting Chen, Zarana Parekh, Hieu Pham, Quoc V. Le, Yun-Hsuan Sung, Zhen Li, and Tom Duerig. Scaling up visual and vision-language representation learning with noisy text supervision. In *ICML*, 2021. 2

- [30] Ye Jia, Yu Zhang, Ron J. Weiss, Quan Wang, Jonathan Shen, Fei Ren, Zhifeng Chen, Patrick Nguyen, Ruoming Pang, Ignacio López-Moreno, and Yonghui Wu. Transfer learning from speaker verification to multispeaker text-to-speech synthesis. In *NeurIPS*, 2018. 4
- [31] Mamadou Keita, Wassim Hamidouche, Hessen Bougueffa Eutamene, Abdelmalik Taleb-Ahmed, David Camacho, and Abdenour Hadid. Bi-LORA: A vision-language approach for synthetic image detection. *Expert Systems*, 42(2):e13829, 2025. 2
- [32] Hasam Khalid, Shahroz Tariq, Minha Kim, and Simon S. Woo. FakeAVCeleb: A novel audio-video multimodal deepfake dataset. In *NeurIPS Datasets and Benchmarks Track*, 2021. 2, 4
- [33] Sohail Ahmed Khan and Duc-Tien Dang-Nguyen. CLIPping the deception: Adapting vision-language models for universal deepfake detection. In *ICMR*, 2024. 2
- [34] Yassine El Kheir, Younes Samih, Suraj Maharjan, Tim Polzehl, and Sebastian Möller. Comprehensive layer-wise analysis of SSL models for audio deepfake detection. In *NAACL Findings*, 2025. 2
- [35] Jaehyeon Kim, Jungil Kong, and Juhee Son. Conditional variational autoencoder with adversarial learning for end-to-end text-to-speech. In *ICML*, pages 5530–5540, 2021. 4
- [36] Marcel Klemm, Carlotta Segna, and Anna Rohrbach. Deepfake doctor: Diagnosing and treating audio-video fake detection. *arXiv preprint arXiv:2506.05851*, 2025. 2, 5
- [37] Gil Knafo and Ohad Fried. Fakeout: Leveraging out-of-domain self-supervision for multi-modal video deepfake detection. *arXiv preprint arXiv:2212.00773*, 2022. 2
- [38] Iryna Korshunova, Wenzhe Shi, Joni Dambre, and Lucas Theis. Fast face-swap using convolutional neural networks. In *ICCV*, 2017. 4
- [39] Christos Koutlis and Symeon Papadopoulos. DiMoDif: Discourse modality-information differentiation for audio-visual deepfake detection and localization. *arXiv preprint arXiv:2411.10193*, 2024. 1, 2
- [40] Christos Koutlis and Symeon Papadopoulos. Leveraging representations from intermediate encoder-blocks for synthetic image detection. *arXiv preprint arXiv:2402.19091*, 2024. 2
- [41] Christos Koutlis and Symeon Papadopoulos. AuViRe: Audio-visual speech representation reconstruction for deepfake temporal localization. In *WACV*, 2026. 5, 6, 13
- [42] Kyungbok Lee, You Zhang, and Zhiyao Duan. A multi-stream fusion approach with one-class learning for audio-visual deepfake detection. In *MMSP*, 2024. 1
- [43] Xiaolou Li, Zehua Liu, Chen Chen, Lantian Li, Li Guo, and Dong Wang. Zero-shot fake video detection by audio-visual consistency. In *Interspeech*, 2024. 1, 2
- [44] Yachao Liang, Min Yu, Gang Li, Jianguo Jiang, Boquan Li, Feng Yu, Ning Zhang, Xiang Meng, and Weiqing Huang. SpeechForensics: Audio-visual speech representation learning for face forgery detection. In *NeurIPS*, 2024. 1, 2, 5, 6, 12, 13, 14
- [45] Huan Liu, Zichang Tan, Chuangchuan Tan, Yunchao Wei, Yao Zhao, and Jingdong Wang. Forgery-aware adaptive transformer for generalizable synthetic image detection. In *CVPR*, 2024. 2
- [46] Shuo Liu, Adria Mallol-Ragolta, Emilia Parada-Cabaleiro, Kun Qian, Xin Jing, Alexander Kathan, Bin Hu, and Bjoern W Schuller. Audio self-supervised learning: A survey. *Patterns*, 3(12), 2022. 2
- [47] Weifeng Liu, Tianyi She, Jiawei Liu, Boheng Li, Dongyu Yao, Ziyong Liang, and Run Wang. Lips are lying: Spotting the temporal inconsistency between audio and visual in lip-syncing deepfakes. In *NeurIPS*, 2024. 2, 4
- [48] Pingchuan Ma, Stavros Petridis, and Maja Pantic. End-to-end audio-visual speech recognition with conformers. In *ICASSP*, 2021. 4
- [49] Pingchuan Ma, Alexandros Haliassos, Adriana Fernandez-Lopez, Honglie Chen, Stavros Petridis, and Maja Pantic. Auto-AVSR: Audio-visual speech recognition with automatic labels. In *ICASSP*, 2023. 4
- [50] Juan M. Martín-Doñas and Aitor Álvarez. The Vicomtech audio deepfake detection system based on wav2vec2 for the 2022 ADD challenge. In *ICASSP*, 2022. 2
- [51] Trisha Mittal, Uttaran Bhattacharya, Ritwik Chandra, Aniket Bera, and Dinesh Manocha. Emotions don’t lie: An audio-visual deepfake detection method using affective cues. In *ACM MM*, 2020. 2
- [52] Nicolas M Müller, Pavel Czempin, Franziska Dieckmann, Adam Froggyar, and Konstantin Böttinger. Does audio deepfake detection generalize? *Interspeech*, 2022. 2
- [53] Nicolas M Müller, Nicholas Evans, Hemlata Tak, Philip Sperl, and Konstantin Böttinger. Harder or different? understanding generalization of audio deepfake detection. In *Interspeech*, 2024. 5
- [54] Huy H. Nguyen, Junichi Yamagishi, and Isao Echizen. Exploring self-supervised vision transformers for deepfake detection: A comparative analysis. In *IJCB*, 2024. 2
- [55] Fan Nie, Jiangqun Ni, Jian Zhang, Bin Zhang, and Weizhe Zhang. FRADE: Forgery-aware audio-distilled multimodal learning for deepfake detection. In *ACM MM*, 2024. 1
- [56] Yuval Nirkin, Yosi Keller, and Tal Hassner. FSGAN: Subject agnostic face swapping and reenactment. In *ICCV*, 2019. 4
- [57] Utkarsh Ojha, Yuheng Li, and Yong Jae Lee. Towards universal fake image detectors that generalize across generative models. In *CVPR*, 2023. 1, 2
- [58] Trevine Oorloff, Surya Koppiseti, Nicolò Bonettini, Divyaraj Solanki, Ben Colman, Yaser Yacoob, Ali Shahriyari, and Gaurav Bharaj. AVFF: Audio-visual feature fusion for video deepfake detection. In *CVPR*, 2024. 2, 5, 6, 12
- [59] Maxime Oquab, Timothée Darcet, Théo Moutakanni, Huy Vo, Marc Szafraniec, Vasil Khalidov, Pierre Fernandez, Daniel Haziza, Francisco Massa, Alaaeldin El-Nouby, Mahmoud Assran, Nicolas Ballas, Wojciech Galuba, Russell Howes, Po-Yao Huang, Shang-Wen Li, Ishan Misra, Michael G. Rabbat, Vasu Sharma, Gabriel Synnaeve, Hu Xu, Hervé Jégou, Julien Mairal, Patrick Labatut, Armand Joulin, and Piotr Bojanowski. DINOv2: Learning robust visual features without supervision. *CoRR*, abs/2304.07193, 2023. 2
- [60] Octavian Pascu, Adriana Stan, Dan Oneata, Elisabeta Oneata, and Horia Cucu. Towards generalisable and calibrated synthetic speech detection with self-supervised representations. In *Interspeech*, 2024. 1, 2

- [61] Alessandro Pianese, Davide Cozzolino, Giovanni Poggi, and Luisa Verdoliva. Training-free deepfake voice recognition by leveraging large-scale pre-trained models. In *ACM Workshop on Information Hiding and Multimedia Security*, 2024. 2
- [62] K R Prajwal, Rudrabha Mukhopadhyay, Vinay P. Nambodiri, and C.V. Jawahar. A lip sync expert is all you need for speech to lip generation in the wild. In *ACM MM*, 2020. 4
- [63] Rui Qian, Tianjian Meng, Boqing Gong, Ming-Hsuan Yang, Huisheng Wang, Serge Belongie, and Yin Cui. Spatiotemporal contrastive video representation learning. In *CVPR*, pages 6964–6974, 2021. 2
- [64] Alec Radford, Jong Wook Kim, Chris Hallacy, Aditya Ramesh, Gabriel Goh, Sandhini Agarwal, Girish Sastry, Amanda Askell, Pamela Mishkin, Jack Clark, et al. Learning transferable visual models from natural language supervision. In *ICML*, 2021. 2, 3
- [65] Tal Reiss, Bar Cavia, and Yedid Hoshen. Detecting deepfakes without seeing any. *arXiv preprint arXiv:2311.01458*, 2023. 1, 2, 13
- [66] Tal Reiss, Bar Cavia, and Yedid Hoshen. Detecting deepfakes without seeing any. *CoRR*, abs/2311.01458, 2023. 1
- [67] Andreas Rossler, Davide Cozzolino, Luisa Verdoliva, Christian Riess, Justus Thies, and Matthias Nießner. FaceForensics++: Learning to detect manipulated facial images. In *CVPR*, 2019. 4, 6, 13
- [68] Ramprasaath R Selvaraju, Michael Cogswell, Abhishek Das, Ramakrishna Vedantam, Devi Parikh, and Dhruv Batra. Grad-CAM: Visual explanations from deep networks via gradient-based localization. In *CVPR*, pages 618–626, 2017. 3
- [69] Sahibzada Adil Shahzad, Ammarah Hashmi, Yan-Tsung Peng, Yu Tsao, and Hsin-Min Wang. AV-Lip-Sync+: Leveraging AV-HuBERT to exploit multimodal inconsistency for video deepfake detection. *arXiv preprint arXiv:2311.02733*, 2023. 2
- [70] Bowen Shi, Wei-Ning Hsu, Kushal Lakhotia, and Abdelrahman Mohamed. Learning audio-visual speech representation by masked multimodal cluster prediction. In *ICLR*, 2022. 2, 4
- [71] Oriane Siméoni, Huy V. Vo, Maximilian Seitzer, Federico Baldassarre, Maxime Oquab, Cijo Jose, Vasil Khalidov, Marc Szafraniec, Seungeun Yi, Michaël Ramamonjisoa, Francisco Massa, Daniel Haziza, Luca Wehrstedt, Jianyuan Wang, Timothée Darcet, Théo Moutakanni, Leonel Sentana, Claire Roberts, Andrea Vedaldi, Jamie Tolan, John Brandt, Camille Couprie, Julien Mairal, Hervé Jégou, Patrick Labatut, and Piotr Bojanowski. DINOv3, 2025. 2
- [72] Stefan Smeu, Elisabeta Oneata, and Dan Oneata. DeCLIP: Decoding clip representations for deepfake localization. In *WACV*, 2024. 2
- [73] Stefan Smeu, Dragos-Alexandru Boldisor, Dan Oneata, and Elisabeta Oneata. Circumventing shortcuts in audio-visual deepfake detection datasets with unsupervised learning. In *CVPR*, 2025. 2, 3, 5, 12
- [74] Koushik Srivatsan, Muzammal Naseer, and Karthik Nandakumar. FLIP: Cross-domain face anti-spoofing with language guidance. In *ICCV*, 2023. 2
- [75] H. Tak, M. Todisco, X. Wang, J. Jung, J. Yamagishi, and N. W. D. Evans. Automatic speaker verification spoofing and deepfake detection using wav2vec 2.0 and data augmentation. In *Proc. Odyssey: The Speaker and Language Recognition Workshop*, 2022. 2
- [76] Ruijie Tao, Zexu Pan, Rohan Kumar Das, Xinyuan Qian, Mike Zheng Shou, and Haizhou Li. Is someone speaking? Exploring long-term temporal features for audio-visual active speaker detection. In *ACM MM*, 2021. 12
- [77] Zhan Tong, Yibing Song, Jue Wang, and Limin Wang. Video-MAE: Masked autoencoders are data-efficient learners for self-supervised video pre-training. In *NeurIPS*, 2022. 2, 3
- [78] Tobias Uelwer, Jan Robine, Stefan Sylvius Wagner, Marc Höftmann, Eric Upschulte, Sebastian Konietzny, Maike Behrendt, and Stefan Harmeling. A survey on self-supervised methods for visual representation learning. *Machine Learning*, 114(4):1–56, 2025. 2
- [79] Chenglong Wang, Jiangyan Yi, Jianhua Tao, Haiyang Sun, Xun Chen, Zhengkun Tian, Haoxin Ma, Cunhang Fan, and Ruibo Fu. Fully automated end-to-end fake audio detection. In *Proc. International Workshop on Deepfake Detection for Audio Multimedia*, pages 27–33, 2022. 2
- [80] Gaojian Wang, Feng Lin, Tong Wu, Zhenguang Liu, Zhongjie Ba, and Kui Ren. FSFM: A generalizable face security foundation model via self-supervised facial representation learning. In *CVPR*, 2024. 3
- [81] Jiadong Wang, Xinyuan Qian, Malu Zhang, Robby T. Tan, and Haizhou Li. Seeing what you said: Talking face generation guided by a lip reading expert. In *CVPR*, 2023. 4
- [82] Xin Wang and Junichi Yamagishi. Investigating self-supervised front ends for speech spoofing countermeasures. In *Odyssey 2022: The Speaker and Language Recognition Workshop*, pages 100–106, 2022. 1, 2
- [83] Xuecheng Wu, Heli Sun, Danlei Huang, Xinyi Yin, Yifan Wang, Hao Wang, Jia Zhang, Fei Wang, Peihao Guo, Suyu Xing, et al. HOLA: Enhancing audio-visual deepfake detection via hierarchical contextual aggregations and efficient pre-training. In *ACM MM*, 2025. 1, 2
- [84] Yuankun Xie, Haonan Cheng, Yutian Wang, and Long Ye. Learning a self-supervised domain-invariant feature representation for generalized audio deepfake detection. In *InterSpeech*, pages 2808–2812, 2023. 2
- [85] Zebin You, Xinyu Zhang, Hanzhong Guo, Jingdong Wang, and Chongxuan Li. Are image distributions indistinguishable to humans indistinguishable to classifiers? *CoRR*, abs/2405.18029, 2024. 2
- [86] Wenxuan Zhang, Xiaodong Cun, Xuan Wang, Yong Zhang, Xi Shen, Yu Guo, Ying Shan, and Fei Wang. SadTalker: Learning realistic 3d motion coefficients for stylized audio-driven single image talking face animation. In *CVPR*, 2023. 4
- [87] Hanqing Zhao, Wenbo Zhou, Dongdong Chen, Weiming Zhang, and Nenghai Yu. Self-supervised transformer for deepfake detection. *arXiv preprint arXiv:2203.01265*, 2022. 2
- [88] Bolei Zhou, Aditya Khosla, Agata Lapediza, Aude Oliva, and Antonio Torralba. Learning deep features for discriminative localization. In *CVPR*, 2016. 3
- [89] Yang Zhou, Xintong Han, Eli Shechtman, Jose Echevarria, Evangelos Kalogerakis, and Dingzeyu Li. MakeltTalk:

Speaker-aware talking-head animation. *ACM Trans. Graph.*, 39(6), 2020. 4

- [90] Mingjian Zhu, Hanting Chen, Mouxiao Huang, Wei Li, Hailin Hu, Jie Hu, and Yunhe Wang. GenDet: Towards good generalizations for AI-generated image detection. *CoRR*, abs/2312.08880, 2023. 2

A. Implementation details

Linear probing. We train the linear probing model for 100 epochs with early stopping (training is stopped if the validation loss does not improve for 10 consecutive epochs). We use the Adam optimizer with a learning rate of 10^{-3} . For AV1M, we select a training set of 22972 videos and a validation set of 2527 videos, both sampled from the official training set. For FAVC, we split the entire dataset into 63% training, 7% validation, and 30% test sets and used only the real video real audio (RVRA) and fake video fake audio (FVFA) samples.

Next-token prediction. The training setup for the next-token prediction is similar to the one used for the linear probing experiments. The main difference is that we now anneal the learning rate using a cosine scheduler. The model is trained on 50k real videos randomly sampled from the AV1M training set, using 45k samples for training and 5k for validation. The training set includes the real samples used for training the linear probes.

Audio-video synchronization. For the audio-video synchronization task, we use the publicly released implementation of [73] with its default settings. We use a temporal neighborhood of 30 frames and a learning rate scheduler with a patience of 5 epochs, a reduction factor of 0.1, and a starting learning rate of 10^{-5} . The training set is identical to the one used for the next-token prediction task.

B. Model checkpoints

For AV-HuBERT we use the `self_large_vox_433h` checkpoint which was pretrained on LRS3 and VoxCeleb2 and finetuned on 433 hours of LRS3 samples for the task of visual speech recognition. For CLIP we use the `openai/clip-vit-large-patch14` checkpoint, and for Video MAE the `MCG-NJU/videomae-large`, both which can be found on HuggingFace. For FSFM we use the `FF++_c23_32frames` checkpoint, which was trained on the FaceForensics++ dataset. For Wav2Vec2, we use the `facebook/wav2vec2-xl-s-r-2b` HuggingFace checkpoint of the 2-billion parameters model, which was pretrained on 436k hours of multilingual data. For Auto-AVSR, we use the best models trained on 3,448 hours: LRS3_V_WER19.1 for visual features, LRS3_A_WER1.0 for audio features, LRS3_AV_WER0.9 for multimodal features. For BRAVE n we use the checkpoints from the high-

resource setup, with self-training, finetuned for ASR and VSR, respectively. Input face crops and audio files are extracted using the AV-HuBERT code.

C. Datasets

General preprocessing. We follow the same preprocessing steps used for each backbone network during its pretraining stage. Visual cropping is applied according to the “pre-training content” column in Tab. 1. Specifically, models pretrained on generic visual content use uncropped frames, those pretrained on faces use face-cropped frames, and those pretrained on lips use lip-cropped frames.

DeepfakeEval 2024 preprocessing. We use TalkNet-ASD [76] to identify which segments in an audio-video media file contain a single person speaking. We selected audio-video segments that met these criteria: (i) each video segment that has an associated audio stream; (ii) a video segment should contain a single speaking face that was tracked in every frame. (Some videos had static images or background music instead of speech and these were discarded); (iii) the identified face is larger than $100\text{px} \times 100\text{px}$; (iv) the duration of audio-video segment is between 3 and 60 seconds.

D. Baselines

Randomly initialized models. For the randomly initialized AV-HuBERT models, we keep the same architecture as the pre-trained version. We also adopt the same initialization scheme used when training AV-HuBERT from scratch: BatchNorm and LayerNorm layers start from constant parameters (weights set to 1 and biases to 0), while linear and embedding layers follow a BERT-style initialization, with weights sampled from a normal distribution with mean 0 and standard deviation 0.02. Finally, we preserve the same preprocessing pipeline as in the pre-trained setup, using log filterbanks for audio and mouth crops for the visual stream.

AVFF [58] is a multimodal, two stage deepfake detector. In the first self-supervised stage, the model encodes both the input audio and video with two separate encoders, masks the tokens in a complementary way, predicts the masked ones using the remaining, visible tokens and then reconstructs the original input. This stage helps the model extract meaningful information from both streams and better align the features. In the second stage, the features extracted are used as input for a classifier network which is trained on the task of deepfake detection. For our experiments we finetuned the checkpoint pretrained on Kinetics400, available in the unofficial open version.³

SpeechForensics [44] is an unsupervised method that detects deepfakes by measuring the alignment between audio

³<https://github.com/JoeLeelyf/OpenAVFF>

and video streams. The alignment is computed as the cosine similarity between audio and visual features extracted from a pretrained AV-HuBERT. To account for desynchronizations, which are common in in-the-wild real videos, the authors propose measuring the best alignment score by shifting the streams within a fixed window. For a fair comparison, we use the same set of AV-HuBERT features, as previously used for linear probing. Since audio and visual features sometimes have different lengths, we align them by trimming at the end. We note, however, that the original implementation uses uniform sampling, which yields slightly better performance. In Sec. E.2, we conduct an ablation study on the pooling operation and window size parameters.

AuViRe [41] is a supervised method trained on the task of temporal forgery localization. The model uses rich self-supervised representations (AV-HuBERT features) as input for a 1D CNN. Firstly, the model reconstructs the input features both within and cross modality (for cross modality, only the video features are reconstructed based on audio ones). Then, a classification head is used to detect the per frame manipulations and a regression head to predict the manipulation segment boundaries. The method was trained on two datasets, LAV-DF and AV-Deepfake 1M. In our experiments, we used the checkpoint trained on AV-Deepfake 1M from the official GitHub repository, together with the default parameters.

AVAD [19] is an unsupervised method which focuses on modeling the distribution over delays in real data and detect fakes at test time based on the deviation from norm. This is achieved by training an autoregressor on the distribution over delays predicted by another component: the audio-visual synchronization model. The authors trained these components only on real data. For our experiments, we used the default parameters and checkpoint specified on the official GitHub repository. The checkpoint used was trained on LRS2 and LRS3 datasets.

RealForensics [22] is a supervised two-step method that leverages self-supervised pretraining to improve robustness. In the first step, the objective is to learn temporally dense video representations using a cross-modal student-teacher framework, where each student predicts the output of the other modality’s teacher. The backbones for each modalities consist of convolutional networks with one-block transformer encoder predictors on top. In the second stage, the detector is tasked with predicting the video targets produced by the video teacher from stage 1 for real videos, combined with a cross-entropy minimization loss on both real and fake inputs. This multi-task learning encourages the model to focus on high-level facial dynamics. For our experiments, we use the model trained on FaceForensics++ [67], with additional real samples from LRW [14].

E. Further results

E.1. Average precision results

We complement the results from Tab. 2 and Tab. 4 with average precision (AP) scores reported in Tab. 5 and Tab. 6, respectively.

E.2. Synchronization of pretrained representations

If audio-visual self-supervised features are trained jointly, then they are already aligned to a degree. Here, we investigate how well this pre-existing alignment works for the task of deepfake detection. This contrasts with the additional alignment introduced in Sec. 3.2, which was required when combining representations from different models.

We use audio-only and visual-only features from AV-HuBERT and measure their alignment via cosine similarity. The fakeness score s between the audio features \mathbf{a} and visual features \mathbf{v} is defined as a generalization of [44, 65]:

$$s(\mathbf{a}, \mathbf{v}) = \min_{\delta \in [-\Delta, +\Delta]} \text{pool}_t(-\cos(\mathbf{a}_t, \mathbf{v}_{t+\delta})), \quad (3)$$

where

- δ is a temporal shift that compensates for imperfect synchronization of real video [19]. Allowing moderate shifts can therefore improve discrimination between real and fake samples. We test both strict ($\Delta = 0$) and moderate alignment ($\Delta = 15$), following [44].
- pool aggregates per-frame fakeness scores. We experiment with several pooling strategies: average, min, max, 3rd and 97th percentiles, and a scaled log-sum-exp (with temperature given by the length of the sequence).

Eq. (3) subsumes prior methods as special cases: FACTOR [65] corresponds to $\Delta = 0$ and 97th-percentile pooling; SpeechForensics [44] corresponds to $\Delta = 15$ with average pooling.

Tab. 7 shows results on the four datasets introduced in Sec. 5.1. At a high level, all variants behave similarly when compared to a supervised baseline (linear probing on AV-HuBERT multimodal features): they underperform on AV1M and perform better on AVLips and DFE-2024. If we look closer, and at the two axes, we first see that average pooling, as used in SpeechForensics [44], is rarely optimal. This is especially evident for AV1M, where the max-based pooling variants perform best. This behavior aligns with the nature of the dataset: since AV1M contains local manipulations, max pooling is able to capture these brief artifacts. Interestingly, for AVLips and DFE-2024, it is the minimum pooling that yields consistent (albeit small) gains. Compared to max pooling, which searches for “evidence of fakeness somewhere,” min pooling searches for “evidence of realness anywhere.” This is particularly suitable for real in-the-wild videos, whose synchronization is imperfect and which contain only a few strongly aligned segments.

Model	Modality	A		B		C		D		E		F		G		H		I		J
		Test on FAVC				Test on AV1M				Test on AVLips				Test on DFE-2024				mean OOD		
		FAVC		AV1M		AV1M		FAVC		FAVC		AV1M		DFE		FAVC			AV1M	
		↓	↓	↓	↓	↓	↓	↓	↓	↓	↓	↓	↓	↓	↓	↓	↓		↓	↓
1	AV-HuBERT (A) random	audio	100	99.9	99.1	91.1	55.7	60.2	89.2	85.2	87.1	79.9								
2	AV-HuBERT (V) random	visual	99.0	96.2	52.3	51.3	63.2	59.5	88.4	91.6	88.8	75.1								
3	AV-HuBERT (A)	audio	100	100	100	99.2	55.6	62.9	93.4	89.1	88.9	82.6								
4	Auto-AVSR (ASR)	audio	100	98.4	96.8	51.2	58.3	55.3	93.4	88.6	88.8	73.4								
5	Wav2Vec2	audio	100	100	100	96.5	61.9	64.3	92.5	92.5	91.7	84.5								
6	BRAVEEn (A)	audio	100	100	99.9	88.7	51.2	53.9	94.0	92.4	90.4	79.4								
7	AV-HuBERT (V)	visual	100	99.6	94.7	62.1	98.4	88.6	95.1	92.9	92.8	89.1								
8	Auto-AVSR (VSR)	visual	99.9	98.7	60.3	52.6	86.2	74.3	92.9	88.8	90.3	81.8								
9	FSFM	visual	99.9	95.2	95.5	53.6	83.6	47.1	93.8	94.5	84.3	76.4								
10	CLIP VIT-L/14	visual	100	99.8	96.8	71.5	65.3	60.9	93.8	90.7	85.2	78.9								
11	Video-MAE-large	visual	100	98.1	99.7	61.3	73.9	53.2	89.3	86.9	84.3	76.3								
12	BRAVEEn (V)	visual	100	99.9	94.1	63.7	98.8	96.9	95.3	93.2	95.5	91.3								
13	AV-HuBERT	audio-visual	100	100	99.9	94.9	76.5	82.1	94.7	90.8	88.7	88.8								
14	Auto-AVSR	audio-visual	99.7	97.7	92.8	54.4	63.7	58.4	92.7	85.9	89.1	74.9								

Table 5. Average precision (AP, %) performance of linear probes trained on multiple self-supervised representations.

Model	AV1M			FAVC		
	Sup.	NTP	Sync.	Sup.	NTP	Sync.
<i>Single features</i>						
AV-HuBERT (A)	99.2	91.8	N/A	100	98.8	N/A
Wav2Vec2	96.5	56.4	N/A	100	96.6	N/A
AV-HuBERT (V)	62.1	49.2	N/A	99.6	97.1	N/A
CLIP	71.5	49.7	N/A	99.8	96.8	N/A
<i>Combination of features</i>						
AV-H (A + V) (rand.)	78.3	64.4	50.8	99.8	98.1	96.0
AV-H (A + V)	97.2	83.4	85.7	100	99.5	99.7
AV-H (A) + CLIP	99.2	88.0	50.0	100	98.6	96.1
W2V2 + AV-H (V)	95.7	59.4	85.1	100	98.6	99.6
W2V2 + CLIP	97.0	56.6	50.5	100	97.6	90.7

Table 6. Average precision (AP, %) performance for deepfake detection when training for the two anomaly detection proxy tasks: next-token prediction (NTP) and audio-video synchronization (sync.). Supervised models (sup.) are trained cross-domain (FAVC→AV1M and AV1M→FAVC, respectively). Anomaly detection models are trained on real data only (a subset of VoxCeleb).

In terms of feature alignment by shifting, we see that it does help in certain setups, most notably for DFE-2024.

Layer-wise analysis. We further analyze the representational capabilities of AV-HuBERT features across all 24 transformer layers. This analysis is conducted on the AV1M test set and, using SpeechForensics [44] with its default hyperparameters (average pooling and a shift window of 15). As shown in Fig. 6, performance roughly stabilizes from layer 7, with a small drop at layer 22. Interestingly, the best performance is obtained at layer 9 (68.6%), but the improve-

ment over the last layer is not substantial. Note that the last-layer performance in Fig. 6 (67.1%) is slightly lower than the corresponding value in Tab. 7 (68.1%); for average pooling and $\Delta = 15$ on AV1M); this discrepancy is due to the absence of LayerNorm in the layer-wise analysis.

E.3. Classification head analysis

We compare the linear classifier described in Sec. 3 with a more powerful head: a transformer. The transformer has width 768, 4 layers, 8 attention heads. Representations are projected using a linear layer to the input 768 dimension. To obtain a classification prediction, we use the [CLS] token and project it through a linear layer. The results are displayed in Tab. 8. We observe that, in most cases, the performance obtained by the transformer model is on par with or slightly below that of linear probing. The single notable exception observed occurs on FSFM features when trained on AV1M and tested on FAVC. In this scenario, performance increases significantly from 40.9% AUC to 72.3% AUC.

E.4. Combinations of features

In Fig. 7 we show the results for combinations of features when testing is done on DFE-2024. Compared to Fig. 5 (testing done on FAVC), certain trends are much better highlighted: first, the performance of every model greatly increases when combined with Wav2Vec2 or AV-HuBERT (V); second, the correlations between models' results are weaker, suggesting that the models capture more distinct patterns.

Pooling function	FAVC		AV1M		AVLips		DFE-2024	
	$\Delta = 0$	$\Delta = 15$	$\Delta = 0$	$\Delta = 15$	$\Delta = 0$	$\Delta = 15$	$\Delta = 0$	$\Delta = 15$
average	99.3	100	65.3	68.1	94.8	92.7	62.7	75.6
<i>Maximum variants</i>								
max	99.3	99.1	76.8	76.9	94.8	93.7	61.0	64.9
log-sum-exp	99.4	99.6	76.8	76.9	95.3	94.2	60.8	64.4
percentile-97	99.5	99.4	75.0	80.0	95.4	93.0	61.4	68.8
<i>Minimum variants</i>								
min	98.2	99.3	58.1	56.1	94.0	96.1	66.3	74.4
percentile-3	99.1	99.5	59.9	58.6	95.4	96.4	63.9	75.7
<i>Supervised baseline</i>								
AV-H + linear on FAVC (row 14 Tab. 2)		100		94.5		78.5		58.2

Table 7. AUC performance (%) when directly measuring the alignment of pretrained AV-HuBERT audio and visual features. We evaluate over pooling functions and temporal shifts (Δ), to compensate desynchronizations of real in-the-wild videos. Bold indicates best results in each column except for the supervised baseline (multimodal AV-HuBERT features with a linear classifier trained on the FAVC dataset).

Model	Head	A		B		C		D		E		F		G		H		I		J	
		Test on FAVC				Test on AV1M				Test on AVLips				Test on DFE-2024				mean OOD			
		FAVC		AV1M		AV1M		FAVC		FAVC		AV1M		DFE		FAVC				AV1M	
		\downarrow	\downarrow	\downarrow	\downarrow	\downarrow	\downarrow	\downarrow	\downarrow	\downarrow	\downarrow	\downarrow	\downarrow	\downarrow	\downarrow	\downarrow	\downarrow	\downarrow	\downarrow	\downarrow	\downarrow
<i>Audio features</i>																					
3	AV-HuBERT (A)	L	100.0	100.0	100.0	99.0	50.0	57.2	65.8	49.1	48.3	67.3									
		T	100.0	99.9	99.9	88.8	47.7	53.4	70.2	48.2	55.0	65.5									
4	Auto-AVSR (ASR)	L	99.7	76.0	96.4	50.3	52.9	49.6	63.5	49.4	47.5	54.3									
		T	100.0	80.1	97.3	51.3	46.4	49.4	70.3	51.6	50.4	54.9									
5	Wav2Vec2	L	100.0	99.9	100.0	96.6	51.3	56.3	58.7	62.3	58.6	70.8									
		T	100.0	99.9	100.0	94.2	47.3	56.5	50.6	52.5	58.2	68.1									
<i>Visual features</i>																					
6	AV-HuBERT (V)	L	100.0	95.5	93.7	64.1	98.3	90.5	72.1	63.7	67.7	80.0									
		T	100.0	92.9	93.7	58.6	98.6	88.3	73.8	70.3	61.8	78.4									
7	Auto-AVSR (VSR)	L	97.8	77.5	59.0	51.3	83.3	70.1	64.3	48.7	56.1	64.5									
		T	98.5	75.5	56.9	51.4	83.4	63.4	62.4	46.9	56.2	62.8									
8	FSFM	L	97.1	40.9	95.3	52.7	84.3	36.8	71.7	71.8	43.5	55.0									
		T	98.8	72.3	99.0	47.9	79.8	42.5	70.7	68.5	48.5	59.9									
9	CLIP ViT-L/14	L	99.8	95.2	96.5	71.1	60.3	53.3	73.9	55.6	43.5	63.2									
		T	99.7	96.4	99.2	62.3	57.0	59.1	73.3	55.8	50.2	63.4									
10	Video-MAE-large	L	100.0	70.4	99.8	60.0	71.3	47.2	54.5	45.6	39.3	55.6									
		T	100.0	60.8	100.0	53.0	81.3	56.5	52.9	58.9	41.2	58.6									
<i>Audio-visual features</i>																					
11	AV-HuBERT	L	100.0	99.5	99.9	94.5	78.5	84.4	70.4	58.2	54.3	78.2									
		T	100.0	99.6	99.9	78.6	82.5	76.8	68.9	59.4	55.9	75.5									
12	Auto-AVSR	L	94.7	68.3	91.6	53.2	59.6	54.6	61.2	43.0	49.2	54.7									
		T	99.7	65.5	93.4	51.1	51.8	51.7	66.5	51.3	51.9	53.9									

Table 8. AUC performance (%) when training a linear layer (L) vs. a transformer (T) (indicated in blue) classifier head on top of features.

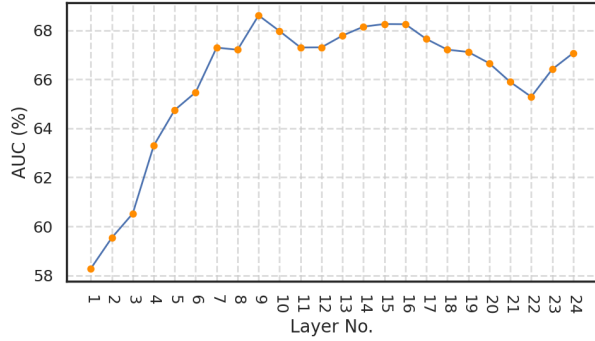


Figure 6. Performance on the AVIM dataset using the pretrained AV-HuBERT representations extracted from different layers. We use the SpeechForensics approach that directly compares AV-HuBERT features over a optimal shifting window.

	Model correlation					AUC	Relative improvement (%)				
W2V2	100.0	44.0	5.8	19.9	19.2	58.6	0.0	-5.2	11.5	-15.9	-11.1
AV-H (A)	44.0	100.0	15.5	10.5	14.7	48.3	14.9	0.0	24.5	-12.8	-7.4
AV-H (V)	5.8	15.5	100.0	6.7	0.3	67.7	-3.5	-11.1	0.0	-29.2	-22.5
V-MAE	19.9	10.5	6.7	100.0	35.8	39.3	25.2	7.1	21.8	0.0	3.0
CLIP	19.2	14.7	0.3	35.8	100.0	43.5	19.8	2.9	20.6	-6.8	0.0
	W2V2	AV-H (A)	AV-H (V)	V-MAE	CLIP		W2V2	AV-H (A)	AV-H (V)	V-MAE	CLIP

Figure 7. Correlations between models (left) and downstream performance (right). Training was done on AVIM, testing on DFEval-2024.